Equilibration of quantum Hall edges in symmetry-broken bilayer graphene

Chandan Kumar, Saurabh Kumar Srivastav, and Anindya Das*
Department of Physics, Indian Institute of Science, Bangalore 560 012, India

(Received 17 July 2018; published 16 October 2018)

Equilibration of quantum Hall edges is studied in a high quality dual gated bilayer graphene device in both unipolar and bipolar regimes when all the degeneracies of the zero energy Landau level are completely lifted. We find that in the unipolar regime when the filling factor under the top gate region is higher than the back gate filling factor, the equilibration is partial based on their spin polarization. However, the mixing of the edge states in the bipolar regime is insensitive to the spin configurations of the Landau levels and the values are very close to the full equilibration prediction. This has been explained by Landau level collapsing at the sharp *p-n* junction in our thin hBN (∼15 nm) encapsulated device, in consistent with the existing theory.

DOI: 10.1103/PhysRevB.98.155421

I. INTRODUCTION

Since the discovery of fractional quantum Hall (QH) effect in two-dimensional electron gas there have been extensive research on the equilibration of edge states to understand their properties [1–3]. Graphene, a single atomic layer of carbons, presents a unique platform where the equilibration of edge states along the *p-n* junction gives rise to fractional values of conductance even in the integer QH regime [4–22]. This is possible because the conduction and valance bands touch each other at the Dirac point, thus selective and control doping combined with the chiral nature of charge carriers can have copropagating edge states along the *p-n* junction interface. This copropagating edge state has been used recently to demonstrate the Mach-Zehnder interferometer in graphene [23], where the selective equilibration between the symmetry-broken QH edges determines the visibility of the interferometer.

Equilibration of edge states have been studied extensively [4–22,24] in graphene in both unipolar and bipolar regimes. The conductance plateaus observed are in agreement with the theoretical prediction by Abanin *et al.* [25]. However, the conductance values in the unipolar regime for broken symmetry states in a graphene device deviates from the predicted equilibration values [25] and were found to be in good match with the partial equilibration based on spin polarized edge states [26]. Similar to graphene, the experiments are also performed on bilayer graphene (BLG), which has even more symmetries like orbital symmetry together with spin and valley symmetries. This leads to a more complex Landau level (LL) phase diagram in BLG, which can be controlled independently by density, electric field, and magnetic field [27–32]. The equilibration experiment performed in BLG [12] also echo with the theory [25]. However, no equilibration study has been performed on the broken symmetry states of ultraclean BLG devices either in a unipolar or bipolar regime.

In this article we report on the equilibration of QH edge states in a high quality dual gated bilayer graphene device in both a unipolar (n-n^*-n/p-p^*-p) and bipolar (n-p^*-n/p-n^*-p) regime when all the degeneracy of the zero-energy LL is lifted. We find that in the unipolar regime when the top gate filling factor (ν_{TG}) is higher than the back gate filling factor (ν_{BG}), the conductance values does not follow the full equilibration prediction [25]. Rather, they follow partial equilibration [26] based on the hierarchical splitting [31,32] of zero energy LL with different spin configuration. Although the partial equilibration based on spin polarization is able to explain most of the conductance values in the unipolar regime, it is still unable to capture the conductance value for all the edge states. The lack of equilibration is better understood by considering the predominant mixing between the nearest edge states. Moreover, in the bipolar regime we find the equilibration of QH edge states for all combinations of ν_{BG} and ν_{TG} irrespective of their spin configurations. The equilibration values are found to be within 10%–15% mismatch from the full equilibration prediction [25]. The equilibration in the bipolar regime is understood in terms of LL collapsing at the sharp *p-n* junction as predicted by Lukose *et al.* [33], NMR Peres *et al.* [34], Gu *et al.* [35], and LaGasse *et al.* [36].

II. DEVICE FABRICATION AND CHARACTERIZATION

The bilayer graphene device is prepared using the dry transfer pick up technique [37] using the following steps. First, a glass slide is prepared with a layer of polydimethylsiloxane (PDMS) and polypropylene carbonate (PPC). This glass slide is used to pick up the desired hBN (∼10–15 nm) flake, which is exfoliated on a silicon wafer. On a separate silicon wafer graphite flakes are exfoliated and a bilayer graphene flake is picked up using the glass slide containing the PDMS, PPC, and hBN. The glass slide containing the heterostructure of PDMS/PPC/hBN/BLG is then transferred onto a thick hBN (∼30 nm) which was already exfoliated on a separate silicon wafer. With this technique graphene remains in its pristine form as it is not exposed to any environmental contaminants or the poly(methyl methacrylate) (PMMA). The

*anindya@iisc.ac.in

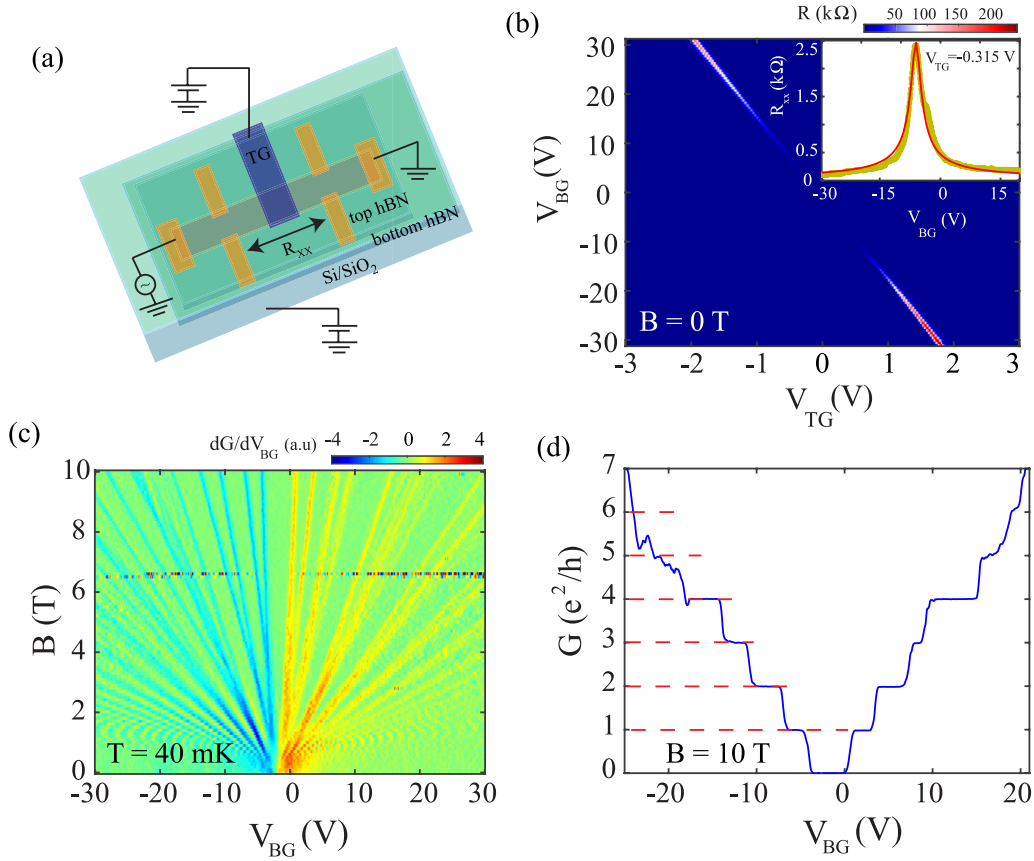

FIG. 1. (a) The schematic of an encapsulated hBN/bilayer graphene/hBN device. The 300-nm-thick SiO_2 acts as a back gate while the top thin hBN acts as a top gate and controls density only in the middle portion of BLG. (b) 2D color plot of resistance as a function of back gate and top gate voltage at $B = 0$ T. The inset shows the resistance at $V_{TG} = -0.315$ V. The red line is fit to resistance to extract mobility. (c) 2D color plot of transconductance dG/dV_{BG} as a function of V_{BG} and perpendicular magnetic field B. Clear Landau levels can be seen emitting from $V_{BG} = -1.3$ V at $B = 0$ T. (d) Two probe resistance as a function of back gate voltage at zero top gate voltage measured at 40 mK and 10 T magnetic field. All the degeneracy of the zero energy Landau level is lifted, leading to the observation of QH plateaus at an integer multiple of e^2/h.

prepared stack of hBN/BLG/hBN is then cleaned in chloroform followed by acetone and isopropyl alcohol (IAP) cleaning. Using the standard lithography technique the contacts are fabricated followed by etching in CHF_3 and O_2 environment. The etch rate is optimized to be 30 nm/min. Soon after etching Cr(3 nm)/Pd(8 nm)/Au(70 nm) is deposited at a base pressure of 3×10^{-7} mbar. The top gate is fabricated by doing another lithography on the prepared stack of hBN/Gr/hBN. The top gate acts as a local gate and controls the density only in the middle portion of the device while the thick SiO_2 acts as a global back gate, controlling the density throughout the device as shown schematically in Fig. 1(a), where the contacts are shown in yellow and the top gate is shown in blue color. The device is 5 μm long, 2 μm wide, and the separation between inner contacts is 2.5 μm.

The conductance is measured using a standard lock-in technique. The different combinations of back gate (V_{BG}) and top gate (V_{TG}) voltages leads to the formation of n-p^*-n/p-n^*-p or n-n^*-n/p-p^*-p region in the same device as shown in Fig. 1(b). The diagonal line in Fig. 1(b) corresponds to the Dirac point under the top gated region, where the density is controlled by both V_{BG} and V_{TG}. From the slope of the diagonal line we calculate a top hBN thickness of ~18 nm. The inset shows resistance measured as a function of V_{BG} for $V_{TG} = -0.315$ V and from the fitting we obtain a mobility of 40,000 cm^2/Vs. Figure 1(c) displays a Landau level fan diagram (dG/dV_{BG}) as a function of V_{BG} and magnetic field (B) at $V_{TG} = 0$ V. Figure 1(d) shows the two probe conductance at $B = 10$ T, where one can clearly see the QH plateaus at an integer multiple of e^2/h suggesting the lifting of spin, valley, and orbital degeneracy of the zero energy LL of BLG.

III. EQUILIBRATION OF QH EDGES

Two probe conductance in the QH regime depends on the back gate (ν_{BG}) and top gate (ν_{TG}) filling factors. This is shown schematically in Fig. 2. The unipolar regime (i.e., top gate and back gate region has same kind of charge carrier) is shown in Figs. 2(a)–2(c). When $\nu_{BG} = \nu_{TG}$, then the current injected from the back gate region completely transmits through the top gate region without any back scattering. For $|\nu_{BG}| > |\nu_{TG}|$, the extra edge states in the back gate region ($|\nu_{BG}| - |\nu_{TG}|$) gets reflected back as shown in Fig. 2(b). Hence the conductance is determined only by the number of edge states under the top gate region and thus, the total

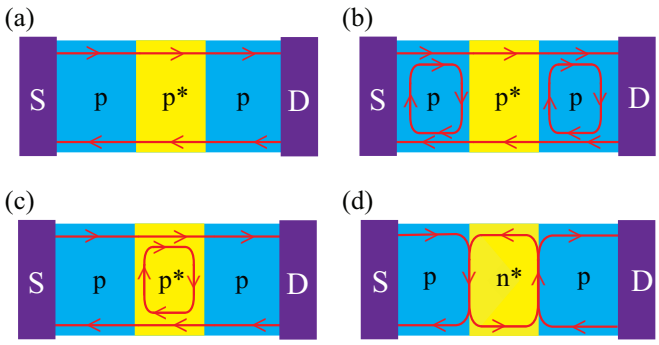

FIG. 2. Schematic of the chiral QH edge state. (a) For $\nu_{BG} = \nu_{TG} = -1$, here, since $|\nu_{BG}| = |\nu_{TG}|$, all the ν_{BG} edge states are completely transmitted through the top gate region. (b) For $|\nu_{BG}| > |\nu_{TG}|$, in this scenario only $|\nu_{TG}|$ edge states are completely transmitted and the rest of the $(|\nu_{BG}| - |\nu_{TG}|)$ edge states gets reflected back. (c) For $|\nu_{BG}| < |\nu_{TG}|$, all the $|\nu_{BG}|$ edge states completely transmitted through the top gate region while the $|\nu_{TG}| - |\nu_{BG}|$ edge states keep circulating in the top gate region. These inner circulating edge states can now interact with the transmitting edge states and the conductance gets modified depending on the equilibration. (d) Since electron and hole edge states have opposite chirality, the electron and hole edge states move copropagating along the *p-n* junction and the full equilibration of these edge states leads to a value of conductance given by Eq. (3).

conductance is given by

$$G_{pp^*p/nn^*n} = \min(|\nu_{BG}|, |\nu_{TG}|)\frac{e^2}{h}. \tag{1}$$

A more interesting situation arises when $|\nu_{TG}| > |\nu_{BG}|$. In this case $|\nu_{BG}|$ edge channels are completely transmitted through the top gate region while $|\nu_{TG}| - |\nu_{BG}|$ number of edges keep circulating under the top gate region. The $|\nu_{BG}|$ edge states transmitting through the top gate region can mix with the circulating $|\nu_{TG} - \nu_{BG}|$ channels under the top gate region, which leads to the modification of two probe conductance. In the case of complete mixing, which has been observed [4–22] on SiO_2 substrate, the conductance is given as

$$G_{pp^*p/nn^*n} = \frac{|\nu_{BG}||\nu_{TG}|}{2|\nu_{TG}| - |\nu_{BG}|}\frac{e^2}{h}. \tag{2}$$

Another interesting scenario arises if the charge carrier in the top gate and the back gate region are of different type; holes and electrons. Since an electron and hole has opposite chirality, the net two probe conductance will be zero unless the clockwise moving QH edge states can equilibrate with the anticlockwise moving edge states along the *p-n* junction interface as shown in Fig. 2(d). For the complete equilibration case the two probe conductance is given as

$$G_{pn^*p/np^*n} = \frac{|\nu_{BG}||\nu_{TG}|}{2|\nu_{TG}| + |\nu_{BG}|}\frac{e^2}{h}. \tag{3}$$

The conductance values discussed so far correspond to the cases when the degeneracy like spin, valley, or orbital are not lifted. A recent experiment [26] by Amet *et al.* studies the equilibration (unipolar regime) in graphene when both the valley and spin degeneracies are completely lifted. In such a scenario they have showed that the equilibration depends

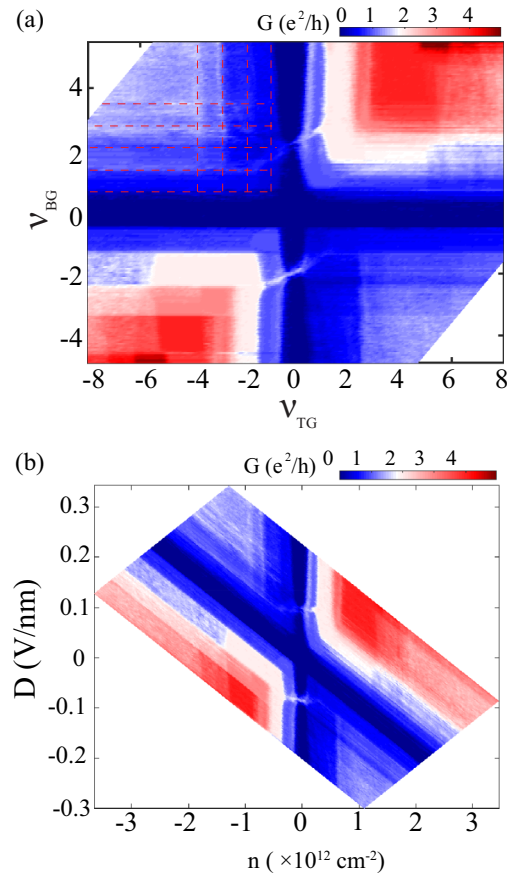

FIG. 3. (a) 2D plot of conductance as a function of ν_{BG} and ν_{TG} at 10 T magnetic field. The horizontal and vertical strips in the unipolar regime corresponds to back gate and top gate filling factor, respectively. Quantized conductance of $2e^2/h$ is observed for $\nu_{BG} = -2$ from $\nu_{TG} = -2$ to $\nu_{TG} = -5$. Similarly for $\nu_{BG} = -4$, quantized conductance of $4e^2/h$ is observed from $\nu_{TG} = -4$ to $\nu_{TG} = -5$. The checkerboard pattern in the bipolar regime is represented by a red dashed line. (b) 2D plot of displacement field as a function of electron density. The LL crossing point is at $D \sim 0.09$ V/nm.

strongly on the spin configuration of the edge states. If the transmitting edge states (ν_{BG}) and inner circulating edge states under the top gate region [Fig. 2(c)] have opposite spin, then the edge state do not equilibrate and hence the conductance is given by $|\nu_{BG}|e^2/h$. On the contrary, if the edge states have the same spin, they equilibrate completely and conductance is given by Eq. (2). Thus, the conductance for a spin polarized edge state in the unipolar regime can be given as [26]

$$G_{\text{partial}} = \sum_{i=\downarrow,\uparrow} \frac{|\nu_{TG,i}||\nu_{BG,i}|}{2|\nu_{TG,i}| - |\nu_{BG,i}|}\frac{e^2}{h}. \tag{4}$$

Here $\nu_{TG,\uparrow}$ ($\nu_{TG,\downarrow}$) refers to the total number of edge states with $\uparrow$ ($\downarrow$), and the same convention holds for ν_{BG}. For example, if $\nu_{BG} = 1$ with $\nu_{BG,\uparrow} = 1$ and $\nu_{TG} = 2$ with $\nu_{TG,\uparrow} = 1$ and $\nu_{TG,\downarrow} = 1$, then $G = 2e^2/3h$. On the other hand, if $\nu_{TG} = 2$ with $\nu_{TG,\downarrow} = 2$ and $\nu_{TG,\uparrow} = 0$, then $G = 0$.

IV. RESULTS

The color plot of two probe conductance as a function of ν_{TG} and ν_{BG} at 10 T is shown in Fig. 3(a). Figure 3(a) is obtained from Fig. 2 of the Supplemental Material (SM) [38], where the conductance is measured as a function of V_{BG} and V_{TG} at 10 T. The back gate and top gate voltages is converted to back gate and top gate filling factors, respectively, using $\nu = \frac{nh}{4eB}$, where n is the density in the system, h is the Plancks constant, e is the electronic charge, and B is the applied magnetic field. The horizontal and vertical strips in Fig. 3(a) corresponds to different ν_{BG} and ν_{TG}, respectively. Interestingly, in the unipolar regime, for $\nu_{BG} = -2$ conductance remains constant at a value of $2e^2/h$ from $\nu_{TG} = -2$ to $\nu_{TG} = -5$. We also observe a similar feature for $\nu_{BG} = -4$, where quantized conductance of $4e^2/h$ is observed from $\nu_{TG} = -4$ to $\nu_{TG} = -5$. On the other hand, in the bipolar regime we observe a clear checkerboard pattern with the conductance values as shown in Table I and compared with the full equilibration case [Eqs. (1)–(3)]. Two lines of higher conductance are also observed connecting the unipolar and bipolar regions. Note that these lines are placed symmetrically about $\nu_{BG} = 0$. Figure 3(b) shows a color plot of conductance as a function of density (n) and displacement field (D). The net density (n) and the displacement field (D) are obtained using the following relations [39]: $n = (D_B - D_T)/e$ and $D = (D_B + D_T)/2$. Here D_B and D_T are the applied back gate and top gate displacement field, respectively. They are given as $D_T = \frac{\epsilon_t(V_{TG} - V_{TG}^{th})}{d_t}$ and $D_B = \frac{\epsilon_b(V_{BG} - V_{BG}^{th})}{d_b}$, where (d_t, d_b) are the thickness of the dielectric layers, (ϵ_t, ϵ_b) are the dielectric constants, and $(V_{TG}^{th}, V_{BG}^{th})$ is the charge neutrality points (CNP) of the device. The higher conductance line joining $\nu_{TG} = -1$ and $\nu_{TG} = 1$ LLs is at $D \sim 0.09$ V/nm. This is consistent with the previous report [27–32], however, we do not see the higher order LL crossing near $D \sim 0$ V/nm as reported in a previous experiment [29].

Figures 4(a)–4(d) plot the cut lines obtained from Fig. 3(a) at different ν_{BG}. In the unipolar regime expected quantized plateaus are observed for $\nu_{TG} = \nu_{BG}$. For $|\nu_{TG}| < |\nu_{BG}|$ also the conductance plateaus agree with Eq. (1) as can be seen in Figs. 4(c) and 4(d). However, for $|\nu_{TG}| > |\nu_{BG}|$ the conductance plateaus are not consistent with the full equilibration prediction as mentioned in Eq. (2). In fact, for $\nu_{BG} = -2$ the conductance plateau remains at $2e^2/h$ from $\nu_{TG} = -2$ to $\nu_{TG} = -5$. Similarly, Fig. 4(d) shows a plateau of $4e^2/h$ from $\nu_{TG} = -4$ to $\nu_{TG} = -5$ for $\nu_{BG} = -4$. For the full equilibration of QH edge states the conductance values of 3/2, 4/3, 5/4 for $\nu_{TG} = -3,\ -4,\ -5$ is expected for $\nu_{BG} = -2$ and a value of $3.33e^2/h$ for $\nu_{BG} = -4$ and $\nu_{TG} = -5$. This gives a very clear signature that some of the edge states, in particular $\nu_{BG} = -2$, prefer not to equilibrate with the circulating edges under the top gate region. The maximum mismatch of 60% is observed for $\nu_{BG} = -2$ and $\nu_{TG} = -5$. Even for $\nu_{BG} = -1$ and $\nu_{BG} = -3$ [Figs. 4(a) and 4(c)] the conductance values obtained in the unipolar regime are higher than the full equilibration prediction. Similar behavior is also observed in the four probe resistance measurement (see SM [38]).

However, the mixing of the edge states in the bipolar regime is insensitive to the spin configurations of the Landau levels. Although the data in the bipolar regime do not show a good plateau as observed in our previous work on single layer graphene [22], its average conductance value is within 10%–15% mismatch from Eq. (3). The measured conductance values in both unipolar and bipolar regimes have been compared with the theoretical prediction based on full equilibration shown in Table I. Each parenthesis in Table I, from left to right, lists the conductance values obtained using full equilibration followed by experimental value. The large mismatch (20%–60%) of conductance observed in the unipolar regime between the theory and experiment is highlighted by a dashed square.

V. DISCUSSIONS

In the following section we try to understand the equilibration data in a unipolar regime. The equilibration of the QH edge state in the unipolar regime can be understood by considering the hierarchical splitting of the zero energy LL [27–32].

The Landau levels (LL) energy in BLG is given by [40,41] $E_n = \pm\hbar\omega\sqrt{N(N-1)}$, where ω is the cyclotron frequency, $\omega = eB/m^*$ and $m^* \sim 0.033m_e$ is the effective mass in BLG, and N is a non-negative integer representing LL index in each layer. For each orbital number N, each of the LL is fourfold degenerate due to two valley and two spin degeneracy. Thus, the zero energy ($N = 0, 1$) LL in BLG is eightfold degenerate [40,42]. Hence, the sequential splitting of the zero energy LL is very intricate. Various efforts have been made to understand the hierarchical splitting of zero energy LL in BLG [27–32].

TABLE I. Conductance values based on full equilibration in unipolar and bipolar regimes (theory; experiment). The deviation in the unipolar regime from the full equilibration prediction is highlighted by a dashed square.

$\nu_{BG}\backslash\nu_{TG}$	-1	-2	-3	-4	-5	1	2	3	4	5
-1	(1; 1.00)	(0.67; 0.80)	(0.6; 0.80)	(0.57; 0.80)	(0.55; 0.80)	(0.33; 0.32)	(0.42; 0.49)	(0.43; 0.51)	(0.44; 0.54)	(0.45; 0.56)
-2	(1; 1.10)	(2; 2.00)	(1.5; 2.00)	(1.33; 2.00)	(1.25; 2.00)	(0.50; 0.51)	(0.66; 0.58)	(0.75; 0.83)	(0.82; 0.96)	(0.83; 0.98)
-3	(1; 1.00)	(2; 2.00)	(3; 3.00)	(2.4; 2.90)	(2.14; 2.90)	(0.60; 0.44)	(0.86; 0.74)	(1.03; 1.10)	(1.09; 1.20)	(1.15; 1.26)
-4	(1; 1.00)	(2; 2.00)	(3; 3.10)	(4; 4.00)	(3.33; 4.00)	(0.67; 0.56)	(1.00; 0.79)	(1.20; 1.12)	(1.33; 1.30)	(1.43; 1.39)

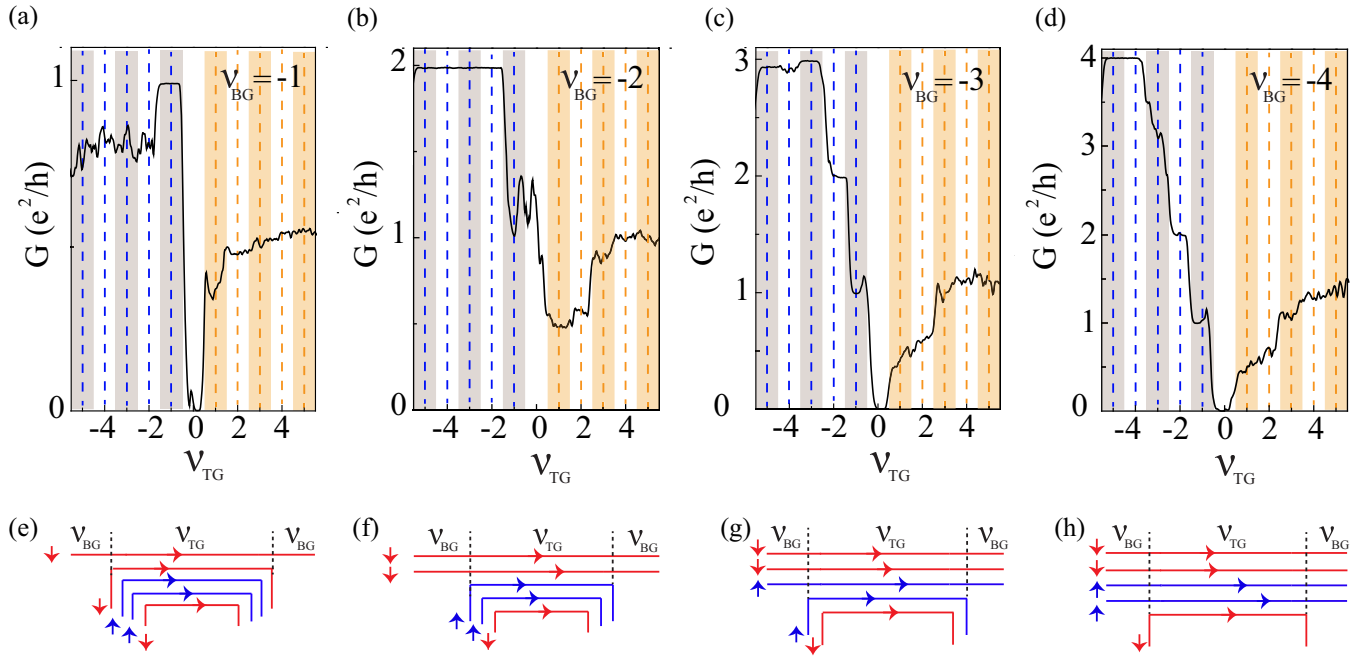

FIG. 4. Line trace of G as a function of ν_{TG} at different set of ν_{BG} at 10 T and 40 mK. (a) Cut across $\nu_{BG} = -1$. (b) Cut across $\nu_{BG} = -2$. (c) Cut across $\nu_{BG} = -3$. (d) Cut across $\nu_{BG} = -4$. For $\nu_{BG} = -2$ ($\nu_{BG} = -4$) conductance remains quantized at $2e^2/h$ ($4e^2/h$) from $\nu_{TG} = -2$ to $\nu_{TG} = -5$ ($\nu_{TG} = -4$ to $\nu_{TG} = -5$), suggesting that these edge states do not equilibrate in our device. Each figure in the lower panel represents the different spin configuration associated with each of the LL. The spin states are obtained from Fig. 5(a) below "b." The up and down spins are represented by blue and red color, respectively. BG and TG in the lower panel represents back gate and top gate region, respectively.

Figure 5(a) shows the model by Zibrov *et al.* [32] and Hunt *et al.* [31] which has been calculated using a four-band tight-binding model [43]. In this model at finite magnetic field both the orbital and spin degeneracy is lifted and the application of a perpendicular electric field lifts the valley degeneracy [31,32].

The other model is shown in Fig. 5(b), where the finite magnetic field only lifts the spin degeneracy and the electric field is responsible for lifting the valley and orbital degeneracy [27–30].

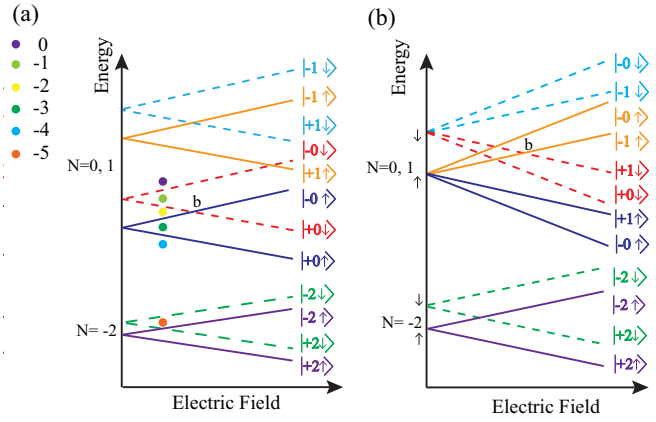

FIG. 5. Schematic representation of LL evolution with magnetic field and the perpendicular electric field. The solid (dashed) line represents the up (down) spin states while the orbital index and valley is represented by (0,1) and (+,−) respectively. (a) Model adapted from Refs. [31,32]. (b) Model adapted from Refs. [27–30]. The filling factors in (a) are indicated for point below "b."

We find that our data can be explained by partial equilibration [Eq. (4)] based on a model presented in Fig. 5(a) [Fig. 5(b)] if the D (electric field) lies below [above] the LL crossing value marked by "b" in Fig. 5(a) [Fig. 5(b)]. The spin configurations are shown in the bottom panel of Fig. 4(b) for the first case. However, it can seen that the higher conductance line at $\nu_{TG} = 0$ in Fig. 3(a) representing the crossing between $\nu_{TG} = -1$ and $\nu_{TG} = 1$ LLs is observed at displacement field $D \equiv D^* = 0.09$ V/nm. It can be also seen from Fig. 3(b) that the displacement field values for $\nu_{BG} = -1$ to -3 and respective $\nu_{TG} = -1$ to -5 lies below D^*. Thus, our equilibration study in the unipolar regime (Figs. 3 and 4) is performed in a region below "b" in Fig. 5. The different spin configuration associated with each LL edge states for D below "b" in Fig. 5(a) is shown elaborately in the bottom row of Fig. 4. The red and blue color denote the up and down spin, respectively.

Table II lists the conductance value obtained using partial equilibration [Eq. (4)] and the experimental data. Each parenthesis in Table II, from left to right, lists

TABLE II. Conductance values based on partial equilibration in a unipolar regime (theory; experiment). The deviation from the partial equilibration model is boldface.

$\nu_{BG}\backslash\nu_{TG}$	−1	−2	−3	−4	−5
−1	(1; 1.00)	**(0.67; 0.80)**	**(0.67; 0.80)**	**(0.67; 0.80)**	**(0.60; 0.80)**
−2	(1; 1.10)	(2; 2.00)	(2; 2.00)	(2; 2.00)	**(1.5; 2.00)**
−3	(1; 1.00)	(2; 2.00)	(3; 3.00)	**(2.67; 2.90)**	**(2.17; 2.90)**
−4	(1; 1.00)	(2; 2.00)	(3; 3.00)	(4; 4.00)	**(3.5; 4.00)**

the conductance value obtained using partial equilibration [Eq. (4)] followed by experimental value. We find that although the partial equilibration model [26] can explain data for $\nu_{BG} = -2$ from $\nu_{TG} = -2$ to $\nu_{TG} = -4$, it fails to explain the quantized conductance value for $\nu_{BG} = -2$ at $\nu_{TG} = -5$ and for $\nu_{BG} = -4$ at $\nu_{TG} = -5$. Moreover, the conductance values obtained at different ν_{TG} for $\nu_{BG} = -1$ and $\nu_{BG} = -3$ are also 20%–30% mismatch with the partial equilibration model. The inconsistency between the values obtained by the partial equilibration model and the experimental data is boldface in Table II, where one can clearly see that experimental values are always higher than the partial equilibration model suggesting lack of equilibration between the transmitting edges and the circulating edges under the top gate region.

The partial equilibration model assumes an equal amount of equilibration between the transmitting edges (ν_{BG}) and the circulating edges ($\nu_{TG} - \nu_{BG}$) under the top gate region depending on their spin polarization irrespective of their spacial location (bottom panel of Fig. 4). The lack of equilibration in our experiment suggests that the equal amount of equilibration between all the edges may not be completely true and possibly the equilibration between the nearest edge states of transmitting edge (ν_{BG}) and circulating edge ($|\nu_{TG}| = |\nu_{BG}| + 1$) in Fig. 4 is stronger compared to innermost circulating edge. For example, when $\nu_{BG} = -2$ the conductance value will be $2e^2/h$ for $\nu_{TG} = -3$ and -4 due to opposite spin configuration, however, for $\nu_{TG} = -5$ the equilibration between $\nu_{BG} = -2$ and $\nu_{TG} = -5$ (same spin polarization) will be very weak as they are spatially separated as well as due to the screening by the inner $\nu_{TG} = -3$ and -4 edges (Fig. 4). Similarly, it can explain Figs. 4(c)–4(g) and Figs. 4(d)–4(h). However, further theoretical studies are required to understand the equilibration of symmetry-broken edges in bilayer graphene, for example the contribution from the orbital and valley degrees freedom.

We now focus on the equilibriation of QH edges in the bipolar regime and the average conductance values shown in Table I, where the values are within 10%–15% mismatch from the predicted values based on full equilibration. It can be also seen that spin polarization is not playing any significant role in the mixing. However, this is not surprising as LaGasse *et al.* [36] have shown that for the ∼40 nm width of the *p-n* junction the Landau levels are superimposed on each other as it is comparable to magnetic length scale and thus, the full mixing of edge states are expected. In our top gated device geometry we estimate the width of the *p-n* junction to be ∼15–20 nm, and thus the edges at the *p-n* junction are not well defined. Not only that, in the bipolar regime strong in-plane electric field is present across our sharp *p-n* junction and studies [33–35] predict the collapse of LL due to the effective higher magnetic length scale. However, further studies are required to understand the exact nature of edge mixing mechanism in BLG.

VI. CONCLUSION

In conclusion, our study provides the experimental evidence of edge state equilibration in bilayer graphene when all the degeneracies of zeroth energy level are completely lifted. Although the partial equilibration based on spin polarization is able to explain most of the conductance values in the unipolar regime, it is still unable to capture them for all the edge states. The lack of equilibration is better understood by considering the predominant mixing between the nearest edges. In the bipolar regime the conductance values are within 10%–15% mismatch from full equilibration model and insensitive to the spin configurations, which has been understood in terms of LL collapsing at the sharp *p-n* junction.

ACKNOWLEDGMENTS

A.D. acknowledges DST Nanomission (Grants No. DST 1470 and No. DST 1597) for the financial support.

[1] C. L. Kane, M. P. A. Fisher, and J. Polchinski, Phys. Rev. Lett. **72**, 4129 (1994).
[2] C. L. Kane and M. P. A. Fisher, Phys. Rev. B **55**, 15832 (1997).
[3] A. Bid, N. Ofek, H. Inoue, M. Heiblum, C. Kane, V. Umansky, and D. Mahalu, Nature (London) **466**, 585 (2010).
[4] J. Williams, L. DiCarlo, and C. Marcus, Science **317**, 638 (2007).
[5] B. Özyilmaz, P. Jarillo-Herrero, D. Efetov, D. A. Abanin, L. S. Levitov, and P. Kim, Phys. Rev. Lett. **99**, 166804 (2007).
[6] G. Liu, J. Velasco, Jr., W. Bao, and C. N. Lau, Appl. Phys. Lett. **92**, 203103 (2008).
[7] T. Lohmann, K. von Klitzing, and J. H. Smet, Nano Lett. **9**, 1973 (2009).
[8] J. Velasco, Jr., G. Liu, W. Bao, and C. N. Lau, New J. Phys. **11**, 095008 (2009).
[9] D.-K. Ki and H.-J. Lee, Phys. Rev. B **79**, 195327 (2009).
[10] D.-K. Ki, S.-G. Nam, H.-J. Lee, and B. Özyilmaz, Phys. Rev. B **81**, 033301 (2010).
[11] J. Velasco, Jr., G. Liu, L. Jing, P. Kratz, H. Zhang, W. Bao, M. Bockrath, C. N. Lau, Phys. Rev. B **81**, 121407 (2010).
[12] L. Jing, J. Velasco Jr., P. Kratz, G. Liu, W. Bao, M. Bockrath, and C. N. Lau, Nano Lett. **10**, 4000 (2010).
[13] M. Woszczyna, M. Friedemann, T. Dziomba, T. Weimann, and F. J. Ahlers, Appl. Phys. Lett. **99**, 022112 (2011).
[14] S.-G. Nam, D.-K. Ki, J. W. Park, Y. Kim, J. S. Kim, and H.-J. Lee, Nanotechnology **22**, 415203 (2011).
[15] J. Velasco, Y. Lee, L. Jing, G. Liu, W. Bao, and C. Lau, Solid State Commun. **152**, 1301 (2012).
[16] A. K. Bhat, V. Singh, S. Patil, and M. M. Deshmukh, Solid State Commun. **152**, 545 (2012).
[17] H. Schmidt, J. C. Rode, C. Belke, D. Smirnov, and R. J. Haug, Phys. Rev. B **88**, 075418 (2013).
[18] N. N. Klimov, S. T. Le, J. Yan, P. Agnihotri, E. Comfort, J. U. Lee, D. B. Newell, and C. A. Richter, Phys. Rev. B **92**, 241301 (2015).

[19] S. Morikawa, S. Masubuchi, R. Moriya, K. Watanabe, T. Taniguchi, and T. Machida, Appl. Phys. Lett. **106**, 183101 (2015).
[20] N. Kumada, F. Parmentier, H. Hibino, D. Glattli, and P. Roulleau, Nat. Commun. **6**, 8068 (2015).
[21] S. Matsuo, S. Takeshita, T. Tanaka, S. Nakaharai, K. Tsukagoshi, T. Moriyama, T. Ono, and K. Kobayashi, Nat. Commun. **6**, 8066 (2015).
[22] C. Kumar, M. Kuiri, and A. Das, Solid State Commun. **270**, 38 (2018).
[23] D. S. Wei, T. van der Sar, J. D. Sanchez-Yamagishi, K. Watanabe, T. Taniguchi, P. Jarillo-Herrero, B. I. Halperin, and A. Yacoby, Sci. Adv. **3**, e1700600 (2017).
[24] W. Long, Q.-f. Sun, and J. Wang, Phys. Rev. Lett. **101**, 166806 (2008).
[25] D. Abanin and L. Levitov, Science **317**, 641 (2007).
[26] F. Amet, J. R. Williams, K. Watanabe, T. Taniguchi, and D. Goldhaber-Gordon, Phys. Rev. Lett. **112**, 196601 (2014).
[27] K. Lee, B. Fallahazad, J. Xue, D. C. Dillen, K. Kim, T. Taniguchi, K. Watanabe, and E. Tutuc, Science **345**, 58 (2014).
[28] A. Kou, B. E. Feldman, A. J. Levin, B. I. Halperin, K. Watanabe, T. Taniguchi, and A. Yacoby, Science **345**, 55 (2014).
[29] P. Maher, L. Wang, Y. Gao, C. Forsythe, T. Taniguchi, K. Watanabe, D. Abanin, Z. Papić, P. Cadden-Zimansky, J. Hone *et al.*, Science **345**, 61 (2014).
[30] B. J. LeRoy and M. Yankowitz, Science **345**, 31 (2014).
[31] B. Hunt, J. Li, A. Zibrov, L. Wang, T. Taniguchi, K. Watanabe, J. Hone, C. Dean, M. Zaletel, R. Ashoori *et al.*, Nat. Commun. **8**, 948 (2017).
[32] A. Zibrov, C. Kometter, H. Zhou, E. Spanton, T. Taniguchi, K. Watanabe, M. Zaletel, and A. Young, Nature (London) **549**, 360 (2017).
[33] V. Lukose, R. Shankar, and G. Baskaran, Phys. Rev. Lett. **98**, 116802 (2007).
[34] N. Peres and E. V. Castro, J. Phys.: Condens. Matter **19**, 406231 (2007).
[35] N. Gu, M. Rudner, A. Young, P. Kim, and L. Levitov, Phys. Rev. Lett. **106**, 066601 (2011).
[36] S. W. LaGasse and J. U. Lee, Phys. Rev. B **94**, 165312 (2016).
[37] L. Wang, I. Meric, P. Huang, Q. Gao, Y. Gao, H. Tran, T. Taniguchi, K. Watanabe, L. Campos, D. Muller *et al.*, Science **342**, 614 (2013).
[38] See Supplemental Material at http://link.aps.org/supplemental/10.1103/PhysRevB.98.155421 for additional data on the optical image of the device, two probe conductance at 10 T, and edge state equilibration in four probe geometry.
[39] Y. Zhang, T.-T. Tang, C. Girit, Z. Hao, M. C. Martin, A. Zettl, M. F. Crommie, Y. R. Shen, and F. Wang, Nature (London) **459**, 820 (2009).
[40] E. McCann and V. I. Fal'ko, Phys. Rev. Lett. **96**, 086805 (2006).
[41] K. S. Novoselov, E. McCann, S. Morozov, V. I. Fal'ko, M. Katsnelson, U. Zeitler, D. Jiang, F. Schedin, and A. Geim, Nat. Phys. **2**, 177 (2006).
[42] F. Guinea, A. H. Castro Neto, and N. M. R. Peres, Phys. Rev. B **73**, 245426 (2006).
[43] J. Jung and A. H. MacDonald, Phys. Rev. B **89**, 035405 (2014).